



Dihedral lattice gauge theories on a quantum annealer

Michael Fromm^{1*}, Owe Philipsen¹ and Christopher Winterowd¹

*Correspondence:

mfromm@itp.uni-frankfurt.de

¹Institut für Theoretische Physik,
Goethe-Universität, Frankfurt am
Main, Germany

Abstract

We study lattice gauge theory with discrete, non-Abelian gauge groups. We extend the formalism of previous studies on D-Wave's quantum annealer as a computing platform to finite, simply reducible gauge groups. As an example, we use the dihedral group D_n with $n = 3, 4$ on a two plaquette ladder for which we provide proof-of-principle calculations of the ground-state and employ the known time evolution formalism with Feynman clock states.

Keywords: Hamiltonian lattice gauge theory; Quantum computing; Quantum annealing

1 Introduction

Lattice gauge theory (LGT) calculations using quantum computers have already seen substantial progress. This is despite the fact that programmable quantum hardware has only recently become widely available to researchers in physics (see e.g. [1] for an up-to-date high-energy physics perspective on the field). With the basic formulation of quantum simulations of LGT being laid out very early on [2], efficient formulations of Abelian [3] and non-Abelian LGT [4, 5] on universal, gate-based hardware now exist. This includes a complete set of instructions for the efficient and accurate simulation of QCD and QED [6].

On the side of adiabatic quantum computing [7], despite the fact that it has been commercially available for more than a decade in the form of quantum annealers (QA) [8], this approach has only recently been used for LGT calculations. These include the pioneering studies on the annealer for the case of $SU(2)$ [9] and $SU(3)$ [10]. In these formulations, the number of qubits necessary to digitize the theory under study scales with the size of the Hilbert space of the problem, which grows exponentially with the spatial volume of the system. Thus, this formulation does not show the expected quantum advantage present in universal, gate-based quantum computing. On the other hand, systems in a QA architecture, such as D-Wave's `Advantage_system5.1`, already comprise several thousand physical qubits [11]. Even at this stage of hardware development, proof-of-principle quantum computations in LGT [9, 10] or other field theories [12] are feasible. The intrinsic nature of the formulation of problems on the annealer simply requires the mapping of the

© The Author(s) 2023. **Open Access** This article is licensed under a Creative Commons Attribution 4.0 International License, which permits use, sharing, adaptation, distribution and reproduction in any medium or format, as long as you give appropriate credit to the original author(s) and the source, provide a link to the Creative Commons licence, and indicate if changes were made. The images or other third party material in this article are included in the article's Creative Commons licence, unless indicated otherwise in a credit line to the material. If material is not included in the article's Creative Commons licence and your intended use is not permitted by statutory regulation or exceeds the permitted use, you will need to obtain permission directly from the copyright holder. To view a copy of this licence, visit <http://creativecommons.org/licenses/by/4.0/>.

lattice field theory onto an optimization problem represented by the Hamiltonian

$$H(q) = \sum_i Q_{ii}q_i + \sum_{i<j} Q_{ij}q_iq_j, \tag{1}$$

with a real, upper-triangular matrix Q and binary variables $q_i \in \{0, 1\}$. This type of problem goes under the name of quadratic unconstrained binary optimization (QUBO). Thus, QA can be seen as an ideal entry point into the field of quantum simulation of LGT. It is in this spirit, that we turn to the subject of our study.

On the lattice, the gauge field Hilbert space is infinite for compact Lie groups and a truncation of the full symmetry becomes necessary (see [13] for a basic overview). One such truncation is the approximation of the full symmetry group by a discrete subgroup, a strategy whose varied success and intricacies are well summarized in [14]. Here, we take the practical approach by choosing the finite, non-Abelian dihedral group D_n as our gauge group, which can be digitized without truncation as in [15]. By mapping this problem onto an optimization problem amenable to the QA, we extend the previous studies of compact Lie groups [9, 10] to the case of simply reducible, finite groups for which we provide the adapted framework. This will allow future studies to separately understand the effects of Hilbert space truncation and comparisons of classical versus quantum simulations. Moreover, our Hamiltonian formulation has connections with gate-based methods. These approaches do not depend on the size of the Hilbert space and thus show polynomial scaling in the spatial volume with the full quantum advantage.

2 Hamiltonian D_n lattice gauge theory

We begin by introducing the Hamiltonian formulation of D_n lattice gauge theory. Our approach closely follows that of [2], where the Hamiltonian approach was worked out for a general gauge group G . As usual, we work on a cubic lattice of dimension d , with the gauge fields living on the links between the lattice sites. The gauge field Hilbert space, denoted by \mathcal{H}_G , is a direct product of the individual link spaces $\mathcal{H}_G = \bigotimes_{\ell} \mathcal{H}_{\ell}$ which, in the group element basis, are defined by $\mathcal{H}_{\ell} = \text{span}(\{|g\rangle\}_{g \in G})$. We start by defining the link operator \hat{U} , acting on \mathcal{H}_{ℓ} , as

$$\hat{U}_{mn}^j = \int dg D_{mn}^j(g) |g\rangle \langle g|, \tag{2}$$

where j labels the irreducible representations (irreps) of G and $D_{mn}^j(g)$ are the Wigner representation matrices for $g \in G$. The indices m, n label the multiplicity of the left and right projection of the link, respectively. This object is of primary importance in the Hamiltonian formulation as it is responsible for the interactions.

The Hamiltonian formulation for $G = \text{SU}(2)$ lattice gauge theory was first written down in [16]. In later work, it was shown how this Hamiltonian could be obtained from the transfer matrix [17]. For a general gauge group G , the lattice Hamiltonian, commonly referred to as the Kogut-Susskind Hamiltonian, consists of two terms

$$\hat{H}_{\text{KS}} = \hat{H}_E + \hat{H}_B, \tag{3}$$

where the first term is referred to as the electric part and the second term is referred to as the magnetic part. The magnetic part takes the form

$$\hat{H}_B = -\lambda_B \sum_{\vec{x}, i < j} \text{Re Tr } \hat{U}_i(\vec{x}) \hat{U}_j(\vec{x} + \hat{i}) \hat{U}_i^\dagger(\vec{x} + \hat{j}) \hat{U}_j^\dagger(\vec{x}), \tag{4}$$

where the sum is over the spatially-oriented plaquettes¹ and can be seen to be diagonal in the group elements basis by virtue of the definition in Eq. (2). In this basis, the electric term, \hat{H}_E , has a form that depends on whether G is taken to be a compact Lie group or a finite group [18, 19]. It is often much more convenient to work in the representation basis, labeled by the states $|jmn\rangle$. Here j labels the irrep and m, n run over the states within the multiplet. In this basis \hat{H}_E becomes diagonal

$$\hat{H}_E = \lambda_E \sum_{\vec{x}} \sum_{i=1}^d \sum_{jmn} f_j |jmn\rangle_{\vec{x},i} \langle jmn|_{\vec{x},i}. \tag{5}$$

The group element basis is related to the representation basis through the following relation

$$\langle g | jmn \rangle = \sqrt{\frac{\text{dim}(j)}{|G|}} D_{mn}^j(g), \tag{6}$$

where $|G|$ is the order of the finite group G . From here on out, we will assume that we are working with finite groups and our formulae will reflect this. Using the transformation in Eq. (6), one can easily transform between the two bases.

It is important to discuss the couplings in the Kogut-Susskind Hamiltonian. The relationship between the couplings λ_E, λ_B appearing in front of the electric and magnetic terms, respectively, can be determined in the limit $a_0 \rightarrow 0$ when deriving the Hamiltonian in the transfer matrix formalism. However, this procedure depends on the gauge group under consideration. While for a compact Lie group, $\lambda_E = g_H^2/2, \lambda_B = 1/g_H^2$, for a finite group it has been determined by previous studies that one should use $\lambda_E = \exp(-2/g_H^2), \lambda_B = 1/g_H^2$, instead [18, 19]. Here we have introduced the Hamiltonian coupling g_H , which is the geometric mean of the spatial and temporal couplings, g_s and g_t . These are introduced in the transfer matrix formulation when one takes the temporal and spatial lattice spacings to be distinct. The coefficients f_j appearing in Eq. (5) are the eigenvalues of the quadratic Casimir operator for the case of compact Lie groups [2]. For example, when $G = \text{SU}(2)$, one gets the familiar result $f_j = j(j + 1)$. On the other hand, for finite gauge groups, the f_j can be derived systematically from the transfer matrix in the limit of vanishing temporal lattice spacing, $a_0 \rightarrow 0$ [19]. Other choices for the coefficients for the case of discrete gauge groups also exist in the literature [20].

2.1 Computation of H_{ij}

With the Kogut-Susskind Hamiltonian given in operator form Eq. (3), there still remains the task of constructing the states of the physical Hilbert space \mathcal{H}_P . The label physical here

¹For the case of $G = D_3, D_4$ which we will consider in this work, we take the link operators to be in the faithful, two-dimensional irrep, which we denote by 2.

refers to the subspace of the larger Hilbert space \mathcal{H}_G that respects local gauge invariance. Formally, in the group element basis, local gauge invariance can be expressed with the help of left and right multiplication operators given by $\Theta_g^L(\vec{x}, i)$ and $\Theta_g^R(\vec{x}, i)$ that act as follows

$$\Theta_g^L|h\rangle = |g^{-1}h\rangle, \quad \Theta_g^R|h\rangle = |hg^{-1}\rangle, \quad g, h \in G, \tag{7}$$

with $\Theta_g^{R\dagger} = \Theta_{g^{-1}}^R$. As usual, the link transforms in the adjoint representation under a gauge transformation. Thus, a local gauge transformation at the site \vec{x} parametrized by g is given by

$$\tilde{\Theta}_g(\vec{x}) \equiv \prod_{i=1}^d \Theta_g^L(\vec{x}, i) \Theta_g^{R\dagger}(\vec{x} - \hat{i}, i). \tag{8}$$

For a generic physical state $|\psi\rangle$, gauge invariance demands

$$\tilde{\Theta}_g(\vec{x})|\psi\rangle = |\psi\rangle, \quad \forall \vec{x} \in \mathbb{Z}^d. \tag{9}$$

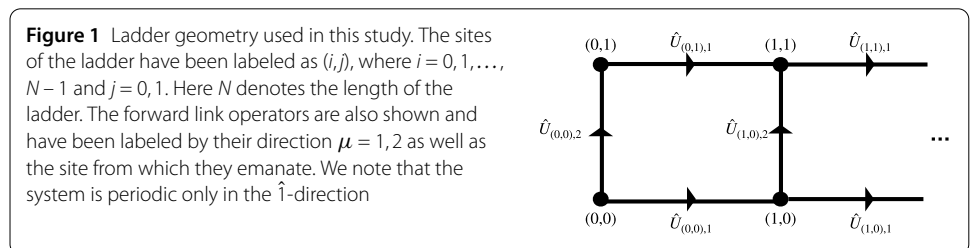
In the representation basis, the statement of Gauss’s law in Eq. (9) is equivalent to $|\psi\rangle$ being written as a direct product of color singlets at each lattice site

$$|\psi\rangle = \bigotimes_{\vec{x}} |00\rangle_{\vec{x}}, \tag{10}$$

where we refer to Appendix B for the details regarding the explicit construction of $|00\rangle_{\vec{x}}$ in terms of the $|jmn\rangle$.

As we are ultimately interested in mapping our system onto a quantum annealer, we are restricted to a rather small system size (Fig. 1). For a given lattice geometry, we are then left with the task of determining the matrix elements of the Hamiltonian (3). We start by introducing the trivial vacuum state $|0\rangle$ with every link ℓ in the trivial representation, $j_\ell = 0$, s.t. $\hat{H}_E|0\rangle = 0$. Physically, this corresponds to the situation where the links contain zero chromoelectric flux. Following the approach of [2], the states of the physical Hilbert space can be systematically generated from this configuration by subsequently acting with gauge-invariant operators. To carry out this procedure, one needs to know how an individual link operator acts on a general state in the representation basis, $|jmn\rangle$. Using the definition of the link operator in (2) and the matrix element in (6), one obtains

$$\hat{U}_{m'n'}^2|jmn\rangle = \sqrt{\frac{\dim(j)}{|G|}} \sum_{g \in G} D_{m'n'}^2(g) D_{mn}^j(g) |g\rangle. \tag{11}$$



This can be further simplified by using the Clebsch-Gordan (CG) series for the tensor product of two arbitrary representation matrices, which yields the result

$$\hat{U}_{m'n'}^2 |jmn\rangle = \sum_J \sum_M \sum_N \sqrt{\frac{\dim(j)}{\dim(J)}} \times \langle 2m'jm|JM\rangle \langle JM|2n'jn\rangle |JMN\rangle, \tag{12}$$

where the sum on J is over the irreps and the sums over M and N are over the states in a given irrep.²

Applying gauge invariant operators repeatedly to the trivial vacuum state with the help of Eq. (12), the enumeration of the configuration space can be performed. In this procedure, Gauss’s law is imposed at each step. This is equivalent to the Wigner 3J-symbol being nonzero for a tuple of irreps, (j_1, j_2, j_3) , which characterize the three links involving a given lattice site. For more details regarding the 3J symbols and Gauss’s law we refer the reader to Appendices A.3 and B.

This task of mapping out the physical Hilbert space can be automated using a Markov-chain-like approach. For this, all one needs are the 3J symbols for the given gauge group G . The total number of states in the full Hilbert space is $\tilde{N}_{\text{irreps}}^{3N}$ states, where $\tilde{N}_{\text{irreps}}$ is the total number of irreps of the gauge group G and N is the size of the ladder. Although enforcing local gauge invariance removes a large number of these states, the physical Hilbert space still grows quite rapidly. In Table 1, we display the size of the physical Hilbert space, where $G = D_3, D_4$. These counts show that even for modest system sizes and small non-Abelian groups there are constraints as to the problems that can be mapped to the quantum annealer.

Once we have enumerated the states in the physical Hilbert space, we can finally compute the matrix elements of the Hamiltonian in this basis. As \hat{H}_E is diagonal in the representation basis, the application of Eq. (5) to the generic state in (56) is trivial. The magnetic Hamiltonian, which is responsible for the interactions, has a nontrivial action on a physical state. To illustrate this, we first write an arbitrary plaquette operator on the ladder

$$\hat{P}_{\vec{x}} = \sum_{n_1, \dots, n_4} \hat{U}_{\vec{x}, 1; n_1, n_2} \hat{U}_{\vec{x} + \hat{1}, 2; n_2, n_3} \times \hat{U}_{\vec{x} + \hat{2}, 1; n_3, n_4} \hat{U}_{\vec{x}, 1; n_4, n_1}, \tag{13}$$

where $\vec{x} = (x, 0)$, $x = 0, \dots, N - 1$ denotes the vertex at the bottom left corner of the plaquette and the sum is over the group indices. Here we label each link by its site vector and

Table 1 List of the size of the physical Hilbert space, N_{conf} , on a ladder of size N for D_3 and D_4 . The configurations are enumerated by a set of integers $\{j_i, i = 1, 2, \dots, 3N\}$ characterizing the irrep of each link on whereby Gauss’s law is satisfied at each site

N	2	3	4
D_3	49	251	$O(1300)$
D_4	76	392	$O(2500)$

²We note that for our choice of the 2 irrep of D_3 and D_4 Eq. (25), the link operators satisfy $U_{m,n}^{2\dagger} = U_{n,m}^2$.

direction. Now, using the relation Eq. (12), we can determine the result of the plaquette operator acting on a state. The matrix element of Eq. (13) between two arbitrary physical states is given by

$$\begin{aligned}
 \langle \psi' | \hat{P}_{\vec{x}} | \psi \rangle &= \sum_{n_1, \dots, n_4} \sum_{\{m_{i,1}, o_{i,1}\}} \cdots \sum_{\{m_{i,n_s}, o_{i,n_s}\}} \\
 &\times \prod_s \begin{pmatrix} j_{\ell_{1,s}} & j_{\ell_{2,s}} & j_{\ell_{3,s}} \\ m_{1,s} & m_{2,s} & m_{3,s} \end{pmatrix} \overline{\begin{pmatrix} l_{\ell_{1,s}} & l_{\ell_{2,s}} & l_{\ell_{3,s}} \\ o_{1,s} & o_{2,s} & o_{3,s} \end{pmatrix}} \\
 &\times \prod_{i \in \mathcal{L}_{\vec{x}}} \delta_{l_i, \tilde{j}_i} \delta_{m_{R_i}, o_{R_i}} \delta_{m_{L_i}, o_{L_i}} \\
 &\times \frac{\sqrt{\dim(j_{\tilde{l}_1}) \dim(j_{\tilde{l}_2}) \dim(j_{\tilde{l}_3}) \dim(j_{\tilde{l}_4})}}{\sqrt{\dim(l_{\tilde{l}_1}) \dim(l_{\tilde{l}_2}) \dim(l_{\tilde{l}_3}) \dim(l_{\tilde{l}_4})}} \\
 &\times \langle 2n_1 j_{\tilde{l}_1} m_{L_{\tilde{l}_1}} | l_{\tilde{l}_1} o_{L_{\tilde{l}_1}} \rangle \langle l_{\tilde{l}_1} o_{R_{\tilde{l}_1}} | 2n_2 j_{\tilde{l}_1} m_{R_{\tilde{l}_1}} \rangle \\
 &\times \langle 2n_2 j_{\tilde{l}_2} m_{L_{\tilde{l}_2}} | l_{\tilde{l}_2} o_{L_{\tilde{l}_2}} \rangle \langle l_{\tilde{l}_2} o_{R_{\tilde{l}_2}} | 2n_3 j_{\tilde{l}_2} m_{R_{\tilde{l}_2}} \rangle \\
 &\times \langle 2n_3 j_{\tilde{l}_3} m_{L_{\tilde{l}_3}} | l_{\tilde{l}_3} o_{L_{\tilde{l}_3}} \rangle \langle l_{\tilde{l}_3} o_{R_{\tilde{l}_3}} | 2n_4 j_{\tilde{l}_3} m_{R_{\tilde{l}_3}} \rangle \\
 &\times \langle 2n_4 j_{\tilde{l}_4} m_{L_{\tilde{l}_4}} | l_{\tilde{l}_4} o_{L_{\tilde{l}_4}} \rangle \langle l_{\tilde{l}_4} o_{R_{\tilde{l}_4}} | 2n_4 j_{\tilde{l}_4} m_{R_{\tilde{l}_4}} \rangle,
 \end{aligned} \tag{14}$$

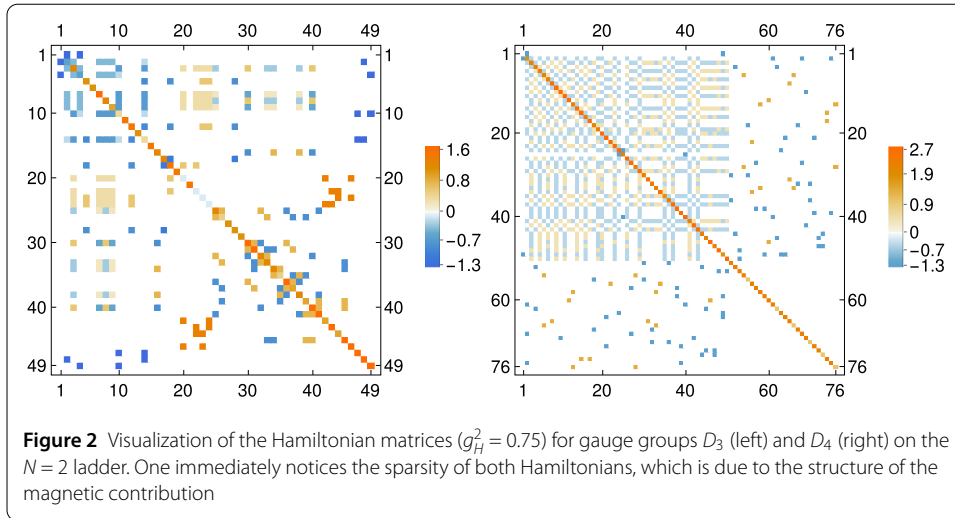
where we refer to $|\psi\rangle$ and $|\psi'\rangle$ as the “in” and “out” states, $\mathcal{L}_{\vec{x}} = \{\tilde{l}_1, \tilde{l}_2, \tilde{l}_3, \tilde{l}_4\}$ denotes the set of all links involved in (13), and the bar denotes complex conjugation. The sums over n_i run over the states in the 2 representation and the sums over $m_{i,\mu}, o_{i,\mu}$ run over the states in the corresponding irreps for each link in the “in” and “out” states. In Eq. (14), we have introduced the Wigner $3j$ symbols which can be generalized to D_n . This along with other details regarding the group theory of D_n are given in Appendix A, with the full derivation of Eq. (14) in Appendix C. Using this result for the plaquette matrix element, one can construct the magnetic Hamiltonian by recalling that $\hat{H}_B = -\lambda_B \sum_{\vec{x}} \hat{P}_{\vec{x}}$. We note here that this construction is completely general and applies to a ladder of arbitrary length.

For the gauge groups which we have examined, it turns out that the Hamiltonian matrix is extremely sparse. This will work to our advantage later on when we map our problem to the quantum annealer. In Fig. 2, we display a visualization of the sparsity of the Hamiltonian for both D_3 and D_4 . Examining the product of delta functions in Eq. (14), the sparseness of the Hamiltonian ultimately comes from the orthonormality of the link states in the representation basis. Once one has calculated the Hamiltonian matrix, the classical part of the calculation is practically complete. In the following, we discuss how our lattice gauge Hamiltonian is transformed into an optimization problem so that the quantum computation on the annealer can be performed.

3 Implementation and results

3.1 Groundstate via variational formulation

Quantum annealing is a method used to solve a very specific type of problem: the calculation of the ground state of a generalized Ising model [11]. Thus, unlike the case of the gate-based approach where one has at one’s disposal a set of universal quantum gates, for



quantum annealing one must cast the problem that one would like to solve into the form of an Ising model.

In the context of lattice gauge theory, it has been shown that one can map the Hamiltonian in Eq. (3) onto a model with QUBO form, Eq. (1), in order to compute the low-lying states of the spectrum [9, 10]. To see how this emerges we consider the variational principle from quantum mechanics

$$E_0 \leq \frac{\langle \psi | \hat{H} | \psi \rangle}{\langle \psi | \psi \rangle}, \tag{15}$$

where E_0 is the ground-state energy. Here we use a variational ansatz with a trial wave function

$$|\psi\rangle = \sum_{\alpha=1}^{N_{\text{conf}}} a_{\alpha} |\phi_{\alpha}\rangle, \tag{16}$$

with real parameters a_{α} and basis states $|\phi_{\alpha}\rangle$ corresponding to the configurations of the physical Hilbert space. The expansion parameters are, in general, complex but here can be chosen to be real as the Hamiltonian is a real, symmetric matrix. It is in this way that solving for the ground-state energy of our lattice Hamiltonian can be recast as an optimization problem as one seeks to minimize $\langle \psi | \hat{H} | \psi \rangle$. Our accuracy in determining the eigenstates of the system is limited only by the precision to which we can determine the coefficients a_{α} . To cast our problem in the form of Eq. (1), we do the following. First, the coefficients are given a fixed-point binary representation. Second, the norm of the wave function is discouraged from being zero by adding a penalty term. Incorporating both of these into our variational calculation, the rhs of Eq. (15) can be rewritten as a cost function

$$F = \langle \psi | \hat{H} | \psi \rangle - \eta \langle \psi | \psi \rangle = \sum_{\alpha, \beta}^{N_{\text{conf}}} \sum_{ij}^K Q_{\alpha\beta, ij} q_{\alpha, i} q_{\beta, j}, \tag{17}$$

where

$$\begin{aligned}
 Q_{\alpha\beta,ij} &= 2^{i+j-2K-2z}(-1)^{\delta_{iK}+\delta_{jK}}h_{\alpha\beta} + \delta_{\alpha\beta}\delta_{ij}\tilde{Q}_{\alpha,i}, \\
 \tilde{Q}_{\alpha,i} &= 2^{i-K-z+1}(-1)^{\delta_{iK}}\sum_{\gamma}^{N_{\text{conf}}}a_{\gamma}^{(z)}h_{\gamma\alpha}, \\
 h_{\alpha\beta} &= H_{\alpha\beta} - \eta\delta_{\alpha\beta}.
 \end{aligned} \tag{18}$$

Here, η represents the tunable parameter multiplying the penalty term. In addition to giving the variational parameters a floating-point representation, in the above definitions we have already introduced the parameter z , which is used in the adaptive variational search method [10]. This procedure iteratively improves the estimates for the $a_{\alpha}^{(z+1)}$ by distributing the K sampling points around the preceding solution to the QUBO problem, $a_{\alpha}^{(z)}$,

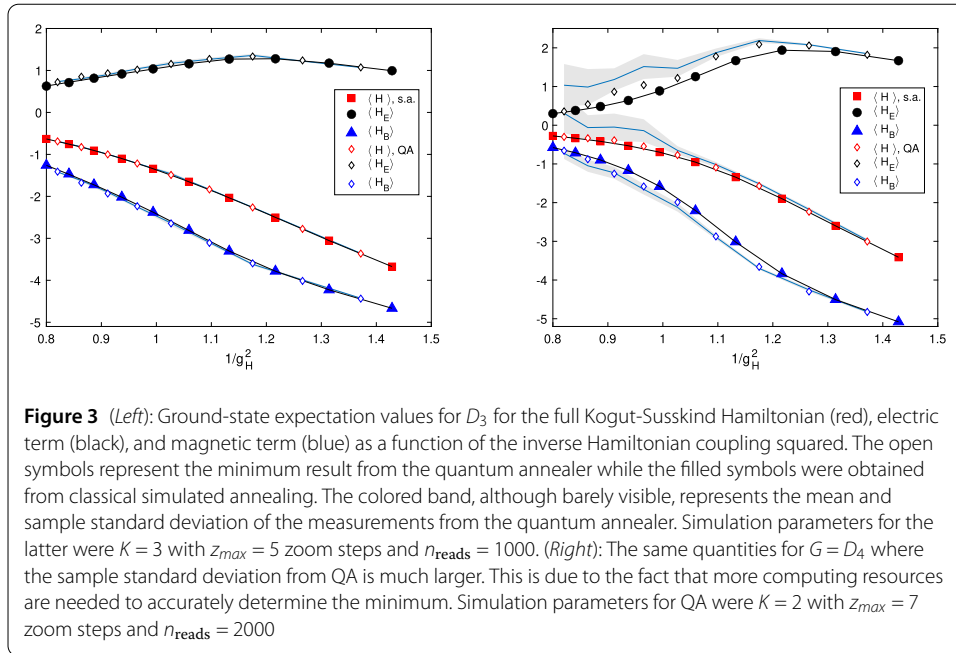
$$a_{\alpha}^{(z+1)} = a_{\alpha}^{(z)} - \frac{q_{\alpha,K}}{2^z} + \sum_{i=1}^{K-1} \frac{q_{\alpha,i}}{2^{K-i+z}}, \tag{19}$$

starting at $a_{\alpha}^{(0)} = 0$. The estimate for the eigenstate is refined at each step, hence the name “zooming” for this procedure. The number of zoom steps plays a significant role in the overall computational cost of our calculation, as each refinement requires calls to the quantum annealer.

The quantum computations are done on the quantum annealing hardware Advantage_system5.1 from D-Wave [11], which is accessible via its API D-Wave Ocean [21]. As our system sizes are still small (c.f. Table 1), the results can be compared with the exact solution using the Hamiltonian Eq. (3) as well as with simulated annealing via the Ocean package `neal`. As alternative, which we did not employ, D-Wave offers hybrid solvers s.a. the `KerberosSampler` [21] that attempt to break down the original QUBO matrix into smaller pieces to be subsequently solved using classical or quantum hardware. This appears to be particularly useful for system sizes that cannot be embedded on currently available annealer architectures.

It should be noted that for computations employing both simulated and quantum annealing, results still have a η dependence, see Eq. (18). As already noticed in [9, 10], convergence to the true ground-state is achieved for η lying in the actual vicinity of the ground-state energy, E_0 (approaching from above). For practical reasons, one can determine the “suitable” η for a given Q by solving Eq. (18) iteratively in η , terminating the calculation when a certain convergence criterion, s.a. relative improvement in the solution, is fulfilled. This strategy works well for local computations with simulated annealing and could in principle be employed also for quantum annealing. Here, runtime on the quantum annealer is the major constraint.

We finally comment on our setup when accessing the annealer via the provided software package. We use the quantum annealer in its forward annealing mode with default annealing schedule and annealing time $t_f = 20\mu\text{s}$. At least one more parameter needs to be provided by the user during the quantum annealing computations. This is what is referred to as the chain strength. For our calculations, we find automatic chain strength tuning (default option) to be sufficient. Figure 3 shows results from both simulated and



quantum annealing, for the ground-state energy $\langle H \rangle$ (red) as well as the expectation value for the magnet part $\langle H_B \rangle$ (blue) and kinetic part $\langle H_E \rangle$ (black) for $G = D_3$ (left). When going to $G = D_4$ (right), an increase in computational resources is needed due to the more complicated energy landscape for the larger group, which we however only partially meet due to runtime restrictions.

3.2 Time evolution

One of the main motivations for working in the Hamiltonian formulation of lattice gauge theories is the ability to access real-time dynamics. This stands in stark contrast to mainstream lattice calculations which work in Euclidean space and must perform an analytic continuation of numerical data in order to access real-time physics. In the gate-based approach, the so-called Trotter approximation is employed to the time evolution operator, $\hat{U}(T) = \exp\{-iT\hat{H}\}$, which evolves an initial state by a finite time T [15]. This approximation consists of replacing the full \hat{U} with products of operators which evolve the system on a smaller time interval, δt . Corrections to this approximation typically scale with powers of δt . This approach to time-evolution of quantum states allows for an efficient simulation of the theory using universal quantum computers.

In order to solve this problem on the quantum annealer, however, one must reformulate time evolution as an optimization problem. This can be done by the introduction of Feynman clock states [22], a mechanism first applied to quantum chemistry calculations in order to generate parallel-in-time quantum dynamics [23]. We thus have to introduce an ancillary quantum system with states $|t\rangle$, $t = 1, 2, \dots, N_t$ where N_t is the number of timeslices in the time evolution. Tensoring this orthonormal state with our as-yet-unknown state vector $|\psi_t\rangle$ at each timeslice, the problem of time evolution is equivalent to the minimization of the following functional

$$\mathcal{L} = \sum_{t,t'=1}^{N_t} \langle t' | \langle \psi_{t'} | \hat{C} | \psi_t \rangle | t \rangle - \eta \left(\sum_{t,t'=1}^{N_t} \langle t' | \langle \psi_{t'} | \psi_t \rangle | t \rangle - 1 \right), \quad (20)$$

where

$$\hat{C} \equiv \hat{C}_0 + \frac{1}{2} (\mathbb{I} \otimes |t\rangle\langle t| + \mathbb{I} \otimes |t+1\rangle\langle t+1| - \hat{U}_{\delta t} \otimes |t+1\rangle\langle t| - \hat{U}_{\delta t}^\dagger \otimes |t\rangle\langle t+1|). \tag{21}$$

Here $\delta t \equiv T/N_t$ is the step size in time, η is a Lagrange multiplier analogous to our previous penalty term, and \hat{C}_0 selects a predetermined initial state. By construction, \hat{C} is hermitian. One can show that the minimum of the functional Eq. (20) corresponds to the exact time-evolved state at each step. Thus, as a result of a single optimization problem one obtains the full time-evolution of a many-body quantum state over a finite time interval. From this functional one can now obtain the QUBO matrix. As previously discussed for the case of finding the ground state of our Hamiltonian, this is what the quantum annealer requires as input. Our discussion closely follows the derivation of [10]. Using a variational state $|\psi_t\rangle|t\rangle$ at each time step t , the functional in Eq. (20) becomes

$$\mathcal{L} = \sum_{\alpha\beta} a_\alpha^* L_{\alpha\beta} a_\beta, \tag{22}$$

where the expansion parameters a_α are complex, the indices in the sum run over all $N_t N_{\text{conf}}$ values, and $L_{\alpha\beta}$ are the matrix elements of the functional. The terms in the above sum can be written in terms of the real and imaginary parts of both $L_{\alpha\beta}$ and a_α . Using the fixed-point representation for both the real and imaginary parts of a_α , one obtains the following QUBO matrix

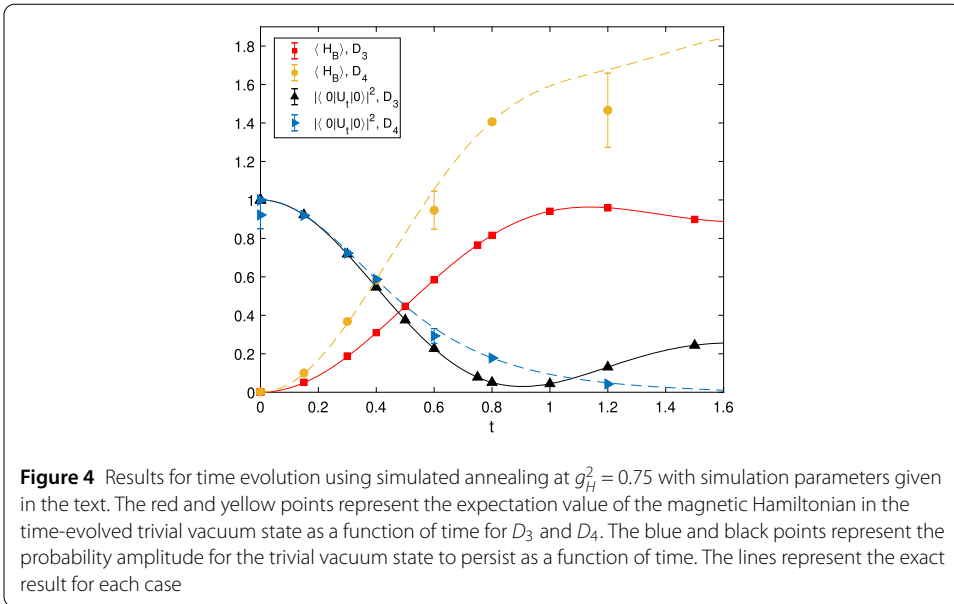
$$Q_{\alpha, i; \beta, j} = \begin{cases} 2^{i+j-2K-2z} (-1)^{\delta_{iK} + \delta_{jK}} \Re L_{\alpha\beta} + 2\delta_{\alpha\beta} \delta_{ij} 2^{i-K-z} (-1)^{\delta_{iK}} \\ \quad \times \sum_\gamma (\Re a_\gamma^{(z)} \Re L_{\gamma\beta} + \Im a_\gamma^{(z)} \Im L_{\gamma\beta}), & 1 \leq i, j \leq K, \\ -2^{i+j'-2K-2z} (-1)^{\delta_{iK} + \delta_{j'K}} \Im L_{\alpha\beta}, & 1 \leq i, j' \leq K, \\ 2^{i'+j-2K-2z} (-1)^{\delta_{i'K} + \delta_{jK}} \Im L_{\alpha\beta}, & 1 \leq i', j \leq K, \\ 2^{i'+j'-2K-2z} (-1)^{\delta_{i'K} + \delta_{j'K}} \Re L_{\alpha\beta} + 2\delta_{\alpha\beta} \delta_{i'j'} 2^{i'-K-z} (-1)^{\delta_{i'K}} \\ \quad \times \sum_\gamma (\Im a_\gamma^{(z)} \Re L_{\gamma\beta} - \Re a_\gamma^{(z)} \Im L_{\gamma\beta}), & 1 \leq i', j' \leq K, \end{cases} \tag{23}$$

where the Latin indices now run from 1 to $2K$ to allow for K bits in representing both the real and imaginary parts of the variational parameters and the primed Latin indices are shifted by K . The dimension of this QUBO matrix is $2KN_t N_{\text{conf}} \times 2KN_t N_{\text{conf}}$, which is significantly larger than the one used to determine the eigenstates of the Hamiltonian. This problem size is too large to be fully embedded on current quantum annealers and we revert to local simulated annealing³ to solve it. The results of our time evolution simulations are displayed in Fig. 4 where we have time evolved the trivial vacuum. Shown are the expectation value of the magnetic part, \hat{H}_B , as well as the probability that the trivial vacuum persists, $|\langle 0|U(t)|0\rangle|^2$. One can see good agreement with the exact results.

4 Conclusion and outlook

We have constructed the Hamiltonian formulation of non-Abelian lattice gauge theories for discrete gauge groups D_n . For the concrete examples D_3, D_4 we worked out the Kogut-

³Simulation parameters are $K = 3, N_t = 3, z_{\text{max}} = 11$ and $n_{\text{runs}} = 8000$.



Susskind Hamiltonian as well as the representations of the corresponding Hilbert space basis states in terms of Clebsch-Gordan coefficients. In principle, this construction can be generalized to larger gauge groups and higher dimensionality. By observing Eq. (55), it is clear that a full 2D lattice, which has a coordination number of four, would involve coupling one additional link per site to yield a representation j_l (corresponding to the addition of three angular momenta in $SU(2)$). The natural coefficients arising in this context would then be the Wigner 6j-symbols, also known as the Racah coefficients [24]. For three dimensions, this construction can in principle be repeated. However, in that case it seems advisable to work purely with CG coefficients. As an example, we have shown how to map these simple lattice gauge theories onto a quantum annealer. In doing so, we have been able to compute the spectrum as well as time evolution for both D_3 and D_4 on small lattices. These proof-of-principle results are of course affected by finite-size effects and going to larger system sizes will have significant impact on observables, such as the spectrum of the theory. However, these are accessible using traditional Markov chain Monte Carlo methods (see e.g. [14]).

The main obstacle to simulate both larger groups as well as larger lattices in our approach is the scaling of the physical Hilbert space with increasing lattice and group size. It thus may be helpful to look in other directions in order to utilize the power of the quantum annealer.

One idea to get around the barrier of rapidly expanding Hilbert spaces for the case of continuous groups is to perform a truncation in the number of allowed irreps as was done in earlier studies of $SU(2)$ and $SU(3)$ in the Hamiltonian formulation [4, 5, 9]. This could also be done for D_n , where $n > 4$. A similar truncation procedure would involve both the electric and magnetic terms in the Hamiltonian, and thus one could investigate the effects on the ground-state energy as well as the dynamics of the system.

One further avenue that could be pursued with the annealer is the estimation of tunneling rates and vacuum decay [12, 25]. These non-perturbative processes are fundamental to the understanding of a wide range of phenomena in both high-energy and condensed matter physics. Another possibility is using quantum annealing in state preparation. This

is an important problem faced by gate-based approaches to simulating lattice gauge theories.

Appendix A: The gauge group D_n

In this [Appendix](#) we summarize key facts and properties of the dihedral group, D_n , that are relevant to this work. In particular, we list the irreducible representations for general n , the Clebsch-Gordan coefficients for both D_3 and D_4 , and outline the algorithm for constructing the Wigner 3J-symbols.

A.1 Irreducible representations

One can define the dihedral group as the symmetry group of a regular, n -sided polygon. The symmetry operations are thus, rotation and reflections in the plane in which the polygon resides. The order of the group, denoted by $|D_n|$, is $2n$. We denote the group element which corresponds to rotations by $2\pi/n$ by r and that which corresponds to a reflection about, say, the y -axis by s . These two elements satisfy the following relations

$$r^n = s^2 = e, \quad srs = r^{-1} = r^{n-1}, \tag{24}$$

where e denotes the identity element. Any element of D_n can be uniquely represented either as r^k , $0 \leq k < n$, or as sr^k , $0 \leq k < n$. We now list the irreducible representations (irreps) of D_n for arbitrary n . We recall that a representation of a group is irreducible if it contains no invariant subspaces.

We start with the one-dimensional irreps of the dihedral group. For n even, there are four one-dimensional irreps while for n odd, there are two one-dimensional irreps. This is summarized by the characters listed in [Table 2](#). Two-dimensional irreps of D_n for arbitrary n also exist and are given, in the standard basis, by

$$\rho_s^h(r^j) = \begin{pmatrix} \cos \frac{2\pi hj}{n} & -\sin \frac{2\pi hj}{n} \\ \sin \frac{2\pi hj}{n} & \cos \frac{2\pi hj}{n} \end{pmatrix}, \quad \rho_s^h(sr^j) = \begin{pmatrix} -\cos \frac{2\pi hj}{n} & \sin \frac{2\pi hj}{n} \\ \sin \frac{2\pi hj}{n} & \cos \frac{2\pi hj}{n} \end{pmatrix}, \tag{25}$$

where we require $0 < h < n/2$, where h labels the various irreps. From [\(25\)](#), the characters can be easily read off

$$\chi_h(r^j) = 2 \cos\left(\frac{2\pi hj}{n}\right), \quad \chi_h(sr^j) = 0. \tag{26}$$

These will prove useful when decomposing an arbitrary tensor representation into a direct sum of irreps.

Table 2 Character table for the one-dimensional irreps of D_n . For n even, all four irreps are valid, while for n odd, only the first two rows apply. In discussing D_3 , we will commonly refer to these one-dimensional irreps as the trivial representation, denoted by $\mathbb{1}$, and the σ -representation

	r^k	sr^k
$\chi_1(g)$	1	1
$\chi_2(g)$	1	-1
$\chi_3(g)$	$(-1)^k$	$(-1)^k$
$\chi_4(g)$	$(-1)^k$	$(-1)^{k+1}$

A.2 Clebsch-Gordan coefficients

An important task in many branches of physics is to understand how one decomposes a tensor product of two irreps into a direct sum of irreps. For the case of D_n lattice gauge theory, in order to construct the physical Hilbert space by acting with gauge-invariant loop operators, one must perform exactly this task. We consider two unitary irreps of a group G , ρ^p and ρ^q . In general, the tensor product of these two representations, denoted by $\rho^p \otimes \rho^q$, is reducible. This implies that it is equivalent to a direct sum of unitary irreps, which can be symbolically expressed as

$$\rho^p \otimes \rho^q \approx \sum_r \oplus n_{p,q}^r \rho^r, \tag{27}$$

where $n_{p,q}^r$ is the number of times that the irrep labeled by r appears in the direct sum. It is immediately clear that $n_{p,q}^r$ is symmetric in p and q . The dihedral group D_n is an example of a so-called simply reducible group, where, among other things, $n_r = 0, 1$ [26]. The following analysis is made simpler by the requirement of only working with simply reducible groups, although it can be generalized to groups where the multiplicities can take values larger than one [27].

The Clebsch-Gordan (CG) coefficients can be thought of as a non-singular matrix transformation U , from the direct product basis to the block-diagonal basis. This is expressed by the following relation

$$(\rho^p \otimes \rho^q)U = U\left(\sum_r \oplus n_{p,q}^r \rho^r\right), \tag{28}$$

there U is of the size $d_p d_q \times d_p d_q$, where d_r denotes the size of the irrep r . The CG coefficients are denoted by

$$U_{i,j;r,\alpha,k} \equiv \left(\begin{array}{cc|c} p & q & r \\ i & j & k \end{array} \right), \tag{29}$$

where $i = 1, 2, \dots, d_p, j = 1, 2, \dots, d_q$, and $k = 1, 2, \dots, d_r$. We list here the results for D_3 and D_4 , where in principle, the CG coefficients can be determined for arbitrary n .

A.2.1 D_3

The tensor products of the one-dimensional irreps are straightforward to compute as $n_{1,\sigma}^\sigma = n_{\sigma,\sigma}^1 = n_{1,1}^1 = 1$. We list below the results for the tensor products involving the two-dimensional irrep (labeled as 2)

$$\left(\begin{array}{cc|c} 2 & 1 & 2 \\ m & 1 & l \end{array} \right) = \delta_{ml}, \tag{30}$$

$$\left(\begin{array}{cc|c} 2 & \sigma & 2 \\ m & \sigma & l \end{array} \right) = \epsilon_{ml}, \tag{31}$$

$$\left(\begin{array}{cc|c} 2 & 2 & 1 \\ m & n & 1 \end{array} \right) = \frac{\delta_{mn}}{\sqrt{2}}, \tag{32}$$

$$\begin{pmatrix} 2 & 2 & | & \sigma \\ m & n & & \end{pmatrix} = \frac{\epsilon_{mn}}{\sqrt{2}}, \quad (33)$$

$$\begin{pmatrix} 2 & 2 & | & 2 \\ m & n & & l \end{pmatrix} = \frac{1}{\sqrt{2}}(\delta_{l2}\sigma_{mn}^z - \delta_{l1}\sigma_{mn}^x), \quad (34)$$

where the indices $m, n, l = 1, 2$, enumerating the basis elements of the two-dimensional irrep.

A.2.2 D_4

With the addition of two additional one-dimensional irreps, the case of D_4 is a straightforward extension of the calculations for D_3 . The tensor products of the one-dimensional irreps are summarized by

$$n_{34}^2 = n_{23}^4 = n_{24}^3 = n_{1q}^q = 1, \quad \tilde{q} = 1, 2, 3, 4, \quad (35)$$

where we use the same labeling of the one-dimensional irreps as in Table 2. The CG coefficients for the 2 (two-dimensional) irrep tensored with the various one-dimensional irreps are as follows

$$\begin{pmatrix} 2 & 2 & | & 2 \\ m & & & l \end{pmatrix} = \epsilon_{ml}, \quad (36)$$

$$\begin{pmatrix} 2 & 3 & | & 2 \\ m & & & l \end{pmatrix} = \sigma_{ml}^z, \quad (37)$$

$$\begin{pmatrix} 2 & 4 & | & 2 \\ m & & & l \end{pmatrix} = \sigma_{ml}^x, \quad (38)$$

$$\begin{pmatrix} 2 & 1 & | & 2 \\ m & & & l \end{pmatrix} = \delta_{ml}. \quad (39)$$

The tensor product of the 2 irrep with itself gives a direct sum of all four one-dimensional irreps. The CG coefficients associated with this decomposition are given by

$$\begin{pmatrix} 2 & 2 & | & 1 \\ m & n & & \end{pmatrix} = \frac{\delta_{mn}}{\sqrt{2}}, \quad (40)$$

$$\begin{pmatrix} 2 & 2 & | & 2 \\ m & n & & \end{pmatrix} = \frac{\epsilon_{mn}}{\sqrt{2}}, \quad (41)$$

$$\begin{pmatrix} 2 & 2 & | & 3 \\ m & n & & \end{pmatrix} = \frac{\sigma_{mn}^z}{\sqrt{2}}, \quad (42)$$

$$\begin{pmatrix} 2 & 2 & | & 4 \\ m & n & & \end{pmatrix} = \frac{\sigma_{mn}^x}{\sqrt{2}}. \quad (43)$$

For D_n , $n > 4$, the analysis becomes more involved as multiple two-dimensional irreps appear.

A.3 Wigner 3J-symbols

In order to construct the physical Hilbert space we need to obtain the Wigner 3J-symbols for D_n . Although the construction for $SU(2)$ is familiar to most, it turns out that there exists a generalization to finite groups [28, 29].

Before providing the relevant formulae, we first provide a few key definitions from representation theory which will aid our discussion. We start by considering a generic irrep of a finite group denoted by (ρ, V) , where ρ is a homomorphism from the group G to the general linear group $GL(V)$ acting on the vector space V . To each irrep j we can associate a dual rep, denoted by j^* , which is equivalent to the rep $\{\rho^*(g), \forall g \in G\}$. The irrep j is related to its dual via the so-called duality map Ω^j , which is unitary and commutes with the action of the representation matrices. Furthermore, the duality map has the property that $(\Omega^j)^T = \alpha_j \Omega^j$, where $\alpha_j = \pm 1, 0$ is the Frobenius-Schur (FS) indicator.

We denote the 3J symbol for the irreps of group G labeled by the tuple (j_1, j_2, j_3) by

$$C_{j_1 j_2 j_3; m_1 m_2 m_3} \equiv \begin{pmatrix} j_1 & j_2 & j_3 \\ m_1 & m_2 & m_3 \end{pmatrix}, \tag{44}$$

where the right-hand side uses the familiar notation from $SU(2)$. The cyclic property of the 3J symbol is given by

$$C_{j_1 j_2 j_3; m_1 m_2 m_3} = \alpha_{j_3} C_{j_3 j_1 j_2; m_3 m_1 m_2}, \tag{45}$$

while one can obtain the 3J symbol for the dual of the tuple of irreps using

$$C_{j_3^* j_2^* j_1^*; m_3 m_2 m_1} = \sum_{n_1 n_2 n_3} \overline{C_{j_1 j_2 j_3; n_1 n_2 n_3} \Omega_{n_3 m_3}^{j_3^*} \Omega_{n_2 m_2}^{j_2^*} \Omega_{n_1 m_1}^{j_1^*}}, \tag{46}$$

where the bar represents complex conjugation. Finally, the normalization of the 3J symbol is fixed by requiring

$$\sum_{\{m_i\}, \{n_i\}} \Omega_{m_3 n_3}^{j_3} \Omega_{m_2 n_2}^{j_2} \Omega_{m_1 n_1}^{j_1} C_{j_1 j_2 j_3; m_1 m_2 m_3} C_{j_3^* j_2^* j_1^*; m_3 n_2 n_1} = 1. \tag{47}$$

This guarantees that when we couple three irreps together at a site of our ladder via the 3J symbol, the resulting singlet state will be normalized to one. The duality map as well as the 3J symbol can be constructed for arbitrary irreps by using the algorithm presented in [28].

A.4 D_3

The results for the 3J symbols for D_3 are as follows

$$C_{111} = C_{1\sigma\sigma} = 1, \tag{48}$$

$$C_{122; m_1 m_2} = \begin{pmatrix} \frac{1}{\sqrt{2}} & 0 \\ 0 & \frac{1}{\sqrt{2}} \end{pmatrix}_{m_1, m_2}, \tag{49}$$

$$C_{\sigma 22; m_1 m_2} = \begin{pmatrix} 0 & \frac{i}{\sqrt{2}} \\ \frac{-i}{\sqrt{2}} & 0 \end{pmatrix}_{m_1, m_2}, \tag{50}$$

$$C_{222;m_1m_2m_3} = \begin{pmatrix} \{0, \frac{1}{2}\} & \{\frac{1}{2}, 0\} \\ \{\frac{1}{2}, 0\} & \{0, -\frac{1}{2}\} \end{pmatrix}_{m_1,m_2,m_3}. \tag{51}$$

A.5 D_4

In a similar fashion, one can obtain the 3J symbols for D_4 , which read

$$C_{111} = C_{122} = C_{133} = C_{144} = C_{122} = C_{342} = 1, \tag{52}$$

$$C_{122} = \begin{pmatrix} \frac{1}{\sqrt{2}} & 0 \\ 0 & \frac{1}{\sqrt{2}} \end{pmatrix}_{m_1,m_2}, \quad C_{222} = \begin{pmatrix} 0 & \frac{i}{\sqrt{2}} \\ -\frac{i}{\sqrt{2}} & 0 \end{pmatrix}_{m_1,m_2}, \tag{53}$$

$$C_{322} = \begin{pmatrix} \frac{1}{\sqrt{2}} & 0 \\ 0 & -\frac{1}{\sqrt{2}} \end{pmatrix}_{m_1,m_2}, \quad C_{222} = \begin{pmatrix} 0 & \frac{1}{\sqrt{2}} \\ \frac{1}{\sqrt{2}} & 0 \end{pmatrix}_{m_1,m_2}. \tag{54}$$

Appendix B: Gauss’s law

For the construction of the physical Hilbert space, one must enforce Gauss’s law at each lattice site. This is precisely the expression of local gauge invariance. For the more common case where compact Lie groups are employed, this condition can be written down in terms of the generators of left and right gauge transformations on the links which enter or leave a given site of the lattice. An analogous construction, which can be generalized to discrete groups such as D_n , uses properties of the states characterizing the various irreps. To be more concrete, at each site of our ladder we tensor together the three links which either start or end on that site while summing over the internal degrees of freedom such that it is a singlet. This has a natural expression in terms of the Wigner 3J-symbols, and can be written as follows

$$\begin{aligned} |00\rangle &= \sum_{m_1, \tilde{m}_1} |j_1, m_1; j_1, \tilde{m}_1\rangle \langle j_1, m_1; j_1, \tilde{m}_1 | 0, 0\rangle, \\ &= \sum_{m_1, \tilde{m}_1} \sum_{m_A} \sum_{m_E} |j_A m_A\rangle \otimes |j_E m_E\rangle \otimes |j_1 m_1\rangle \langle j_A, m_A; j_E, m_E | j_1, \tilde{m}_1\rangle \langle j_1, m_1; j_1, \tilde{m}_1 | 0, 0\rangle, \\ &= \sum_{m_1, \tilde{m}_1} \sum_{m_A} \sum_{m_E} (-)^{f(j_A, j_E, j_1; \tilde{m}_1)} |j_A m_A\rangle \otimes |j_E m_E\rangle \otimes |j_1 m_1\rangle \begin{pmatrix} j_A & j_E & j_1 \\ m_A & m_E & \tilde{m}_1 \end{pmatrix} \\ &\quad \times \langle j_1, m_1; j_1, \tilde{m}_1 | 0, 0\rangle, \\ &= \sum_{m_1} \sum_{m_A} \sum_{m_E} (-)^{f(j_A, j_E, j_1; m_1)} |j_A m_A\rangle \otimes |j_E m_E\rangle \otimes |j_1 m_1\rangle \begin{pmatrix} j_A & j_E & j_1 \\ m_A & m_E & m_1 \end{pmatrix}, \end{aligned} \tag{55}$$

where f is a known function which has been tabulated for D_3 and D_4 and takes integer or half-integer values. In the third line we have used the fact that the CG coefficients for the projection of the tensor product of any two irreps onto the trivial representation ($\mathbb{1}$) is diagonal. The expression in (55) is valid for continuous as well as finite groups. Using the Wigner 3J-symbols and the CG coefficients for D_3 and D_4 which were listed in Appendix A, one can produce a gauge invariant state on the ladder by taking the tensor product of the analogous expression at each site. This is represented by the expres-

sion

$$\begin{aligned}
 |\psi\rangle &= \bigotimes_s |00\rangle_s \tag{56} \\
 &= \sum_{\{m_{i,1}\}} \cdots \sum_{\{m_{i,n_s}\}} \left(\bigotimes_{\ell} |j_{\ell} m_{L_{\ell}} m_{R_{\ell}}\rangle \right) \prod_s \begin{pmatrix} j_{\ell_{1,s}} & j_{\ell_{2,s}} & j_{\ell_{3,s}} \\ m_{1,s} & m_{2,s} & m_{3,s} \end{pmatrix} (-)^{f(j_{\ell_{1,s}}, j_{\ell_{2,s}}, j_{\ell_{3,s}}; m_{3,s})},
 \end{aligned}$$

where the $\{m_{i,s}\}$ are the local multiplicities at site s of the link ℓ in representation j_{ℓ} , and in the product over links, each link has multiplicities $m_{L_{\ell}}$ and $m_{R_{\ell}}$ associated with the “left” and “right” ends of the link. One can thus label the states of the Hilbert space by a set of $N_{\text{links}} = 3N$ integers characterizing the irreps, where N is the number of plaquettes, with the condition that at each site there is a valid tuple with nonzero 3J symbol. From here, one has everything one needs in order to enumerate the states in the physical Hilbert space.

Appendix C: Plaquette contribution

Here we provide the details for the matrix element of a plaquette in the physical Hilbert space. This derivation is similar to that of [9] for the case of SU(2). The application of the plaquette in (13) on the arbitrary physical state listed in (56) is given by

$$\begin{aligned}
 \hat{P}_{\bar{x}}|\psi\rangle &= \sum_{n_1, \dots, n_4} \sum_{\{m_{L_i}\}} \sum_{\{m_{R_i}\}} \hat{U}_{\bar{1}; n_1 n_2} |j_{\bar{1}} m_{L_{\bar{1}}} m_{R_{\bar{1}}}\rangle \tag{57} \\
 &\quad \otimes \hat{U}_{\bar{2}; n_2 n_3} |j_{\bar{2}} m_{L_{\bar{2}}} m_{R_{\bar{2}}}\rangle \otimes \hat{U}_{\bar{3}; n_3 n_4} |j_{\bar{3}} m_{L_{\bar{3}}} m_{R_{\bar{3}}}\rangle \\
 &\quad \otimes \hat{U}_{\bar{4}; n_1 n_4} |j_{\bar{4}} m_{L_{\bar{4}}} m_{R_{\bar{4}}}\rangle \bigotimes_{i \in \mathcal{L}_{\bar{x}}} |j_i m_{L_i} m_{R_i}\rangle \\
 &\quad \times \prod_s \begin{pmatrix} j_{\ell_{1,s}} & j_{\ell_{2,s}} & j_{\ell_{3,s}} \\ m_{1,s} & m_{2,s} & m_{3,s} \end{pmatrix} (-)^{f(j_{\ell_{1,s}}, j_{\ell_{2,s}}, j_{\ell_{3,s}}; m_{3,s})}, \tag{58}
 \end{aligned}$$

where the sums over m_{L_i} and m_{R_i} represent $3N$ individual sums whose ranges depend on the configuration of the state $|\psi\rangle$. Using the Clebsch-Gordan series, we can obtain the result of each link operator acting on an arbitrary link state. Applying this to each term in (58) yields

$$\begin{aligned}
 \hat{P}_{\bar{x}}|\psi\rangle &= \sum_{n_1, \dots, n_4} \sum_{\{m_{L_i}\}} \sum_{\{m_{R_i}\}} \prod_s \begin{pmatrix} j_{\ell_{1,s}} & j_{\ell_{2,s}} & j_{\ell_{3,s}} \\ m_{1,s} & m_{2,s} & m_{3,s} \end{pmatrix} (-)^{f(j_{\ell_{1,s}}, j_{\ell_{2,s}}, j_{\ell_{3,s}}; m_{3,s})} \bigotimes_{i \in \mathcal{L}_{\bar{x}}} |j_i m_{L_i} m_{R_i}\rangle \\
 &\quad \otimes \sum_{J_{\bar{1}}} \sum_{M_{L_{\bar{1}}}} \sum_{M_{R_{\bar{1}}}} \sqrt{\frac{\dim(j_{\bar{1}})}{\dim(J_{\bar{1}})}} \langle 2n_1 j_{\bar{1}} m_{L_{\bar{1}}} | J_{\bar{1}} M_{L_{\bar{1}}} \rangle \langle J_{\bar{1}} M_{R_{\bar{1}}} | 2n_2 j_{\bar{1}} m_{R_{\bar{1}}} \rangle \\
 &\quad \times |J_{\bar{1}} M_{L_{\bar{1}}} M_{R_{\bar{1}}}\rangle \\
 &\quad \otimes \sum_{J_{\bar{2}}} \sum_{M_{L_{\bar{2}}}} \sum_{M_{R_{\bar{2}}}} \sqrt{\frac{\dim(j_{\bar{2}})}{\dim(J_{\bar{2}})}} \langle 2n_2 j_{\bar{2}} m_{L_{\bar{2}}} | J_{\bar{2}} M_{L_{\bar{2}}} \rangle \langle J_{\bar{2}} M_{R_{\bar{2}}} | 2n_3 j_{\bar{2}} m_{R_{\bar{2}}} \rangle \\
 &\quad \times |J_{\bar{2}} M_{L_{\bar{2}}} M_{R_{\bar{2}}}\rangle
 \end{aligned}$$

$$\begin{aligned}
& \otimes \sum_{J_{i_3}} \sum_{M_{L_{i_3}}} \sum_{M_{R_{i_3}}} \sqrt{\frac{\dim(j_{i_3})}{\dim(J_{i_3})}} \langle 2n_4 j_{i_3} m_{L_{i_3}} | J_{i_3} M_{L_{i_3}} \rangle \langle J_{i_3} M_{R_{i_3}} | 2n_3 j_{i_3} m_{R_{i_3}} \rangle \\
& \times | J_{i_3} M_{L_{i_3}} M_{R_{i_3}} \rangle \\
& \otimes \sum_{J_{i_4}} \sum_{M_{L_{i_4}}} \sum_{M_{R_{i_4}}} \sqrt{\frac{\dim(j_{i_4})}{\dim(J_{i_4})}} \langle 2n_1 j_{i_4} m_{L_{i_4}} | J_{i_4} M_{L_{i_4}} \rangle \langle J_{i_4} M_{R_{i_4}} | 2n_4 j_{i_4} m_{R_{i_4}} \rangle \\
& \times | J_{i_4} M_{L_{i_4}} M_{R_{i_4}} \rangle. \tag{59}
\end{aligned}$$

We now take the inner product of (59) with a second generic state $|\psi'\rangle$ which satisfies Gauss' law. We note that states in the representation basis are orthonormal

$$\langle j' m' n' | j m n \rangle = \delta_{j'j} \delta_{m'm} \delta_{n'n}, \tag{60}$$

and thus we obtain the result in Eq. (14).

Acknowledgements

The authors would like to thank Brendan Pankovich for useful discussions and Michael Spannowsky for comments on the manuscript.

Funding

Open Access funding enabled and organized by Projekt DEAL. The work is supported by the Deutsche Forschungsgemeinschaft (DFG, German Research Foundation) through the grant CRC-TR 211 "Strong-interaction matter under extreme conditions" – project number 315477589 – TRR 211 and by the State of Hesse within the Research Cluster ELEMENTS (Project ID 500/10.006).

Abbreviations

QCD, Quantum Chromodynamics; QED, Quantum Electrodynamics; API, Application programming interface.

Availability of data and materials

Simulation data are available from the corresponding author upon reasonable request.

Declarations

Ethics approval and consent to participate

Not applicable.

Consent for publication

Not applicable.

Competing interests

The authors declare no competing interests.

Author contributions

All authors contributed equally in the conception phase, CW and MF carried out the computations and simulations. All authors jointly drafted and reviewed the manuscript and approved the submission.

Received: 2 December 2022 Accepted: 14 August 2023 Published online: 25 August 2023

References

- Bauer CW, Davoudi Z, Balantekin AB, Bhattacharya T, Carena M, de Jong WA, Draper P, El-Khadra A, Gemelke N, Hanada M, Kharzeev D, Lamm H, Li Y-Y, Liu J, Lukin M, Meurice Y, Monroe C, Nachman B, Pagano G, Preskill J, Rinaldi E, Roggero A, Santiago DI, Savage MJ, Siddiqi I, Siopsis G, Zanten DV, Wiebe N, Yamauchi Y, Yeter-Aydeniz K, Zorzetti S, editors. Quantum simulation for high energy physics. 2022. [arXiv:2204.03381](https://arxiv.org/abs/2204.03381).
- Byrnes T, Yamamoto Y. Simulating lattice gauge theories on a quantum computer. *Phys Rev A*. 2006;73:022328. <https://doi.org/10.1103/PhysRevA.73.022328>. [arXiv:quant-ph/0510027](https://arxiv.org/abs/quant-ph/0510027).
- Haase JF, Dellantonio L, Celi A, Paulson D, Kan A, Jansen K, Muschik CA. A resource efficient approach for quantum and classical simulations of gauge theories in particle physics. *Quantum*. 2021;5:393. <https://doi.org/10.22331/q-2021-02-04-393>. [arXiv:2006.14160](https://arxiv.org/abs/2006.14160).
- Klco N, Stryker JR, Savage MJ. SU(2) non-Abelian gauge field theory in one dimension on digital quantum computers. *Phys Rev D*. 2020;101:074512. <https://doi.org/10.1103/PhysRevD.101.074512>. [arXiv:1908.06935](https://arxiv.org/abs/1908.06935).

5. Ciavarella A, Klco N, Savage MJ. A trailhead for quantum simulation of SU(3) Yang-Mills lattice gauge theory in the local multiplet basis. *Phys Rev D*. 2021;103:094501. <https://doi.org/10.1103/PhysRevD.103.094501>. [arXiv:2101.10227](https://arxiv.org/abs/2101.10227).
6. Kan A, Nam Y. Lattice quantum chromodynamics and electrodynamics on a universal quantum computer. 2021. [arXiv:2107.12769](https://arxiv.org/abs/2107.12769).
7. Albash T, Lidar DA. Adiabatic quantum computation. *Rev Mod Phys*. 2018;90:015002. <https://doi.org/10.1103/RevModPhys.90.015002>.
8. Johnson MW, Amin MHS, Gildert S, Lanting T, Hamze F, Dickson N, Harris R, Berkley AJ, Johansson J, Bunyk P, Chapple EM, Enderud C, Hilton JP, Karimi K, Ladizinsky E, Ladizinsky N, Oh T, Perminov I, Rich C, Thom MC, Tolkacheva E, Truncic CJ, Uchaikin S, Wang J, Wilson B, Rose G. Quantum annealing with manufactured spins. *Nature*. 2011;473(7346):194–8. <https://doi.org/10.1038/nature10012>.
9. Rahman SA, Lewis R, Mendicelli E, Powell S. SU(2) lattice gauge theory on a quantum annealer. *Phys Rev D*. 2021;104:034501. <https://doi.org/10.1103/PhysRevD.104.034501>. [arXiv:2103.08661](https://arxiv.org/abs/2103.08661).
10. Illa M, Savage MJ. Basic elements for simulations of standard model physics with quantum annealers: multigrid and clock states. 2022. [arXiv:2202.12340](https://arxiv.org/abs/2202.12340).
11. D-Wave. 2022. <https://www.dwavesys.com>.
12. Abel S, Spannowsky M. Observing the fate of the false vacuum with a quantum laboratory. *PRX Quantum*. 2021;2:010349. <https://doi.org/10.1103/PRXQuantum.2.010349>. [arXiv:2006.06003](https://arxiv.org/abs/2006.06003).
13. Zohar E. Quantum simulation of lattice gauge theories in more than one space dimension – requirements, challenges and methods. *Philos Trans R Soc A*. 2021;380:20210069. <https://doi.org/10.1098/rsta.2021.0069>. [arXiv:2106.04609](https://arxiv.org/abs/2106.04609).
14. Alam MS, Hadfield S, Lamm H, Li ACY. Quantum simulation of dihedral gauge theories. 2021. [arXiv:2108.13305](https://arxiv.org/abs/2108.13305).
15. Lamm H, Lawrence S, Yamauchi Y. General methods for digital quantum simulation of gauge theories. *Phys Rev D*. 2019;100:034518. <https://doi.org/10.1103/PhysRevD.100.034518>. [arXiv:1903.08807](https://arxiv.org/abs/1903.08807).
16. Kogut J, Susskind L. Hamiltonian formulation of Wilson's lattice gauge theories. *Phys Rev D*. 1975;11:395–408. <https://doi.org/10.1103/PhysRevD.11.395>.
17. Creutz M. Gauge fixing, the transfer matrix, and confinement on a lattice. *Phys Rev D*. 1977;15:1128–36. <https://doi.org/10.1103/PhysRevD.15.1128>.
18. Harlow D, Ooguri H. Symmetries in quantum field theory and quantum gravity. 2018. [arXiv:1810.05338](https://arxiv.org/abs/1810.05338).
19. Carena M, Lamm H, Li Y-Y, Liu W. Lattice renormalization of quantum simulations. *Phys Rev D*. 2021;104:094519. <https://doi.org/10.1103/PhysRevD.104.094519>.
20. Bender J, Zohar E, Farace A, Cirac JI. Digital quantum simulation of lattice gauge theories in three spatial dimensions. *New J Phys*. 2018;20:093001. <https://doi.org/10.1088/1367-2630/aadb71>. [arXiv:1804.02082](https://arxiv.org/abs/1804.02082).
21. D-Wave Ocean. 2022. <https://docs.ocean.dwavesys.com>.
22. Feynman RP. Quantum mechanical computers. *Opt News*. 1985;11(2):11–20. <https://doi.org/10.1364/ON.11.2.000011>.
23. McClean JR, Parkhill JA, Aspuru-Guzik A. Feynman's clock, a new variational principle, and parallel-in-time quantum dynamics. *Proc Natl Acad Sci*. 2013;110(41):3901–9. <https://doi.org/10.1073/pnas.1308069110>.
24. Messiah A. *Quantum mechanics*. vol. 2. Amsterdam: North-Holland; 1962.
25. Abel S, Chancellor N, Spannowsky M. Quantum computing for quantum tunneling. *Phys Rev D*. 2021;103:016008. <https://doi.org/10.1103/PhysRevD.103.016008>.
26. Wigner EP, Wightman AS, Mehra J. *The collected works of Eugene Paul Wigner*. Berlin: Springer; 1992–1998. <http://www.loc.gov/catdir/enhancements/fy0818/92038376-d.html>.
27. van Den Broek PM, Cornwell JF. Clebsch-Gordan coefficients of symmetry groups. *Phys Status Solidi B*. 1978;90(1):211–24. <https://doi.org/10.1002/pssb.2220900123>.
28. Hu Y-T. Emergent properties in exactly solvable discrete models for two-dimensional topological phases. PhD thesis. University of Utah; 2013. <https://collections.lib.utah.edu/ark:/87278/s6gb5c8b>.
29. Hu Y, Geer N, Wu Y-S. Full dyon excitation spectrum in extended Levin-wen models. *Phys Rev B*. 2018;97:195154. <https://doi.org/10.1103/PhysRevB.97.195154>.

Publisher's Note

Springer Nature remains neutral with regard to jurisdictional claims in published maps and institutional affiliations.

Submit your manuscript to a SpringerOpen[®] journal and benefit from:

- Convenient online submission
- Rigorous peer review
- Open access: articles freely available online
- High visibility within the field
- Retaining the copyright to your article

Submit your next manuscript at ► [springeropen.com](https://www.springeropen.com)
